Neural Network and Machine Learning Allocation of Redundant Controls for Power Optimization on a Compound Helicopter

Jean-Paul Reddinger
Ph.D. Candidate
Rensselaer Polytechnic Institute
Troy, NY

Farhan Gandhi
Professor
Rensselaer Polytechnic Institute
Troy, NY

ABSTRACT

For a compound helicopter with control of main rotor speed, auxiliary propeller thrust, and stabilator pitch; a predictive neural network is trained to estimate power as a function of the redundant control settings for a range of flight speeds using a comprehensive database of 2,335 prior Rotorcraft Comprehensive Analysis System (RCAS) simulations. This neural network can be used as a surrogate model for a gradient based optimization to find the redundant control settings that produce a trim state with a minimized power requirement. The study highlights the importance of modeling relevant constraints (main rotor flapping and control limits), as well as having training data in the same locality that the predictions are being made. For producing accurate results with sparse initial datasets (20 trim states), a process of machine learning is demonstrated, wherein the neural network is iteratively updated using the resulting power from each prior optimization. When used appropriately, both the machine learning and fixed models demonstrate ability to allocate redundant controls such that the power requirement is within 1% – 3% of the true minimum.

NOTATION

H_{in}^{n}	input of the n^{th} neuron of the hidden layer
H_{n}^{out}	output of the n^{th} neuron of the hidden layer
f_D	equivalent flat plate drag area (ft^2)
M_{tip}	advancing blade tip Mach number
P	total vehicle power requirement (hp)
P_{actual}	true power as simulated in RCAS (hp)
$P_{prediction}$	power prediction from a surrogate model (hp)
T_{coll}	collective thrust from the wing-mounted propellers (lbs)
W	weights applied to each neural network connection
α	vehicle pitch attitude (deg)
β	peak azimuthal blade flapping angle (deg)
δ_s	stabilator pitch (deg)
θ_0	blade collective pitch at 75% span (deg)
θ_{1c}	lateral cyclic pitch (deg)
θ_{1s}	longitudinal cyclic pitch (deg)
Ω	main rotor rotational speed, counterclockwise (rad/s)

INTRODUCTION

Conventional rotary-wing aircraft are usually capable of maximum speeds no greater than 150 – 170 kts, limited by the onset of advancing blade compressibility, retreating blade stall, high vibration, and deterioration in rotor performance leading to an eventual inability to produce the forces and moments required to equilibrate the aircraft. One approach to overcome these challenges is to tilt the rotor forward to function as an axial propeller, while transferring the lifting function to wings in forward flight. Tilt-rotor aircraft like the Bell-Boeing V22-Osprey are thereby capable of attaining maximum speeds greater than 275 kts, but have a significantly higher empty-weight fraction, increased complexity, and reduced hover and low-speed performance (Ref. 1).

If the maximum speed requirement is in the 200 – 250 kts range, a lift-offset coaxial configuration with auxiliary propulsion, or a slowed-rotor compound configuration with auxiliary lift and propulsion may be more viable solutions, offering reduced complexity and improved hover performance relative to a tilt-rotor aircraft. Coaxial rotor technology, using two counter-rotating rotors with each generating lift on its advancing side in the high-speed regime, was referred to as the Advancing Blade Concept and first implemented on the Sikorsky XH-59 helicopter in the 1970's (Ref. 2). After a hiatus of several years, Sikorsky Aircraft Corp. developed a second generation high-speed coaxial rotor aircraft prototype, the X2 Technology Demonstrator (Refs. 3–6), which improved on many of the shortcomings of the XH-59. These technologies are also being scaled up by Sikorsky for application to the S-97 Raider, and jointly by Sikorsky and Boeing for the SB>1 Defiant in response to the Armys Joint Multi-Role program (Refs. 7, 8).

While lift-offset coaxial configurations generate lift on the advancing side of each rotor, a slowed-rotor compound helicopter uses a fixed wing to provide the majority of the aircraft lift in high speeds. Efforts focused on the devel-

Presented at the AHS International 73rd Annual Forum & Technology Display, Fort Worth, Texas, USA, May 9–11, 2017.

opment of slowed rotor compound configurations go back several decades, with the AH-56 Cheyenne compound helicopter (Ref. 9) representing a significant milestone in the 1960's, but because of complications in the development and testing phase, the program was canceled. More recently, the Large Civil Tandem Compound (LCTC) was one of the concepts considered under the NASA Joint Heavy Lift Program (Ref. 10). Compound enabling technologies have also been explored, such as Piasecki Aircraft Corporation's Vectored Thrust Ducted Propeller (VTDP), which allowed a modified SH-60 Sea Hawk to operate at speeds greater than 170 kts (Ref. 11). Airbus Helicopter's X3 compounded the AS 365 Dauphin with propellers mounted on wings for auxiliary lift and propulsion at high speed (Ref. 12). It has since set the current speed record of 255 kts for an edgewise rotor.

In addition to the major design and development programs discussed above, many fundamental studies over the years have focused on the performance and benefits of compound helicopters (Refs. 13–22). To contribute to understanding of the aeromechanical behavior of slowed-rotors in high speed flight, a series of wind tunnel experiments were conducted on UH-60A rotors at high advance ratios under the NASA/Army UH-60A Airloads Program (Ref. 23).

Both compound and coaxial helicopter designs supplement the classical helicopter controls with additional control effectors not present on conventional rotorcraft. In the case of compound helicopters, control of the rotor speed, wing flaps and ailerons, stabilator, and auxiliary thrust, provides an opportunity for compound helicopters to exploit control redundancy and fly the aircraft in any number of different ways. For example, the controls could be selected to minimize the power requirement, vibrations, blade flapping, acoustic noise, or some weighted combination thereof, while satisfying vehicle force and moment equilibrium in steady level flight (Refs. 24–30).

In a recent effort, Horn and co-workers simulated an in-flight determination of the optimal control configurations for a high-speed compound aircraft by using Fly-to-Optimal methods (Refs. 31,32). The approach, based on perturbation of a subset of individual controls, requires a substantial amount of time, especially when multiple redundant controls are used, and the solution is itself dependent on the sequence of control perturbations. The Fly-to-Optimal approach makes no use of any prior knowledge of the system in attempting to determine the best compound helicopter controls.

Ref. 33 introduces a knowledge-based method of predicting controls required to maintain trim for a compound helicopter at two discrete flight speeds—hover and 100 kts—with surrogate modeling. The surrogate models are trained on several hundred trim states each, and are shown capable of determine the set of controls which minimize power for each flight speed. This study extends these efforts to a produce a surrogate model capable of allocating controls for minimum power over a continuum of flight speeds, and using a minimal set of trim state data. A pilot or even an assistive auto-pilot could use such a model to inform the most optimal combinations of additional controls not being used by the pilot, such as main rotor collective pitch at high speeds or auxiliary propeller thrust at low speeds.

COMPOUND HELICOPTER MODELING AND ANALYSIS

The compound helicopter model used in the simulations of this study is adapted from a UH-60A rotor and fuselage model, and was also used in Ref. 33. A schematic of the model is shown in Figure 1. Table 1 provides a detailed summary of the compound configuration's major subsystems and their characteristics. The configuration is designed for high speed flight, and the model used is representative of that. Propellers are used to provide thrust in high-speed flight, so the forward shaft tilt present on the UH-60A is removed. Furthermore, the UH-60A twist provides excellent hover performance, but the large non-linear twist results in high negative lift and drag at the advancing blade tips for high advance ratios, so a more moderate $-8°$ twist is considered in this study. Other features of the UH-60A rotor including airfoil selections, chord distribution, and sectional mass and stiffness properties are left unchanged. The airfoil aerodynamic coefficients are interpolated from non-linear lookup tables.

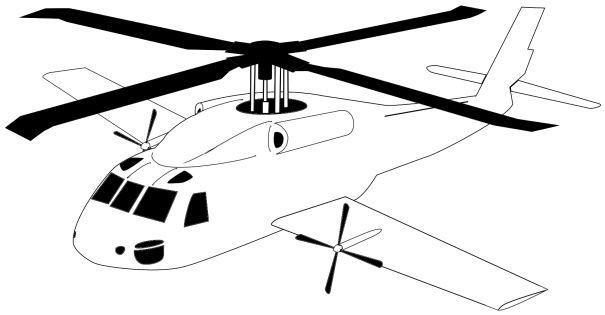

Fig. 1. Compound helicopter schematic

The gross takeoff weight is increased to 20,110 lbs, which is equivalent to the takeoff weight of the Piasecki X-49A SpeedHawk. This increased weight can be assumed to include the weight of the wings, propellers, and any additional weight required to compound the UH-60A airframe. To model fuselage drag, the compounded fuselage is assumed to be more streamlined than the UH-60A fuselage. A UH-60A has a minimum equivalent flat plate drag area of 35.14 ft^2 (Ref. 34). According to trends established by Ormiston (Ref. 19), a modern aircraft at this gross weight that is designed for high speed flight can be expected to have an equivalent flat plate drag area of 18.49 ft^2. The quadratic relation between vehicle pitch attitude and drag as measured for the UH-60A was maintained, resulting in the following expression for the equivalent flat plate drag area as a function of vehicle pitch attitude (in degrees).

$$f_D = 18.487 + 0.0441\alpha^2 \text{ (ft}^2\text{)}$$

Table 1. Compound helicopter configuration

Characteristic	Measurement
Gross Weight	20,110 lbs
C.G. Location	1.5 ft aft, 5.8 ft below hub
Main Rotor	
Rotor Radius	26.8 ft
Nominal Rotor Speed	258 RPM
Nominal Blade Twist	$-8°$
Shaft Tilt	$0°$
Airfoils	SC-1094 R8/SC-1095
Horizontal Stabilizer	
Effective Area	43 ft^2
Airfoil	NACA 0012
Wing	
Planform Area	220 ft^2
Chord	5 ft
Span	44 ft
Incidence Angle	$3.8°$
Aerodynamic Properties	Aerostar FJ-100
C.P. Location	0.5 ft aft, 6.5 ft below hub
Auxiliary Propellers	
Radii	4.5 ft
Speed	1,934 RPM
Solidity	0.12
Locations	10 ft laterally, on each wing

The wing model is based on the three dimensional lift, drag, and moment coefficients for the wing of the Aerostar FJ-100, which is the wing used on the X-49A. For the purpose of the study in Ref. 29, it has been set at an incidence of 3.8°, so that for pitch-level flight at 225 kts it will be flying close its peak L/D of 22.4, and scaled in area from 178.2 ft^2 to 220 ft^2 so that at this attitude it will be lifting about 83% of the gross weight of the aircraft. With only 1.2° of nose-up vehicle pitch, the wings can produce enough aerodynamic lift to completely offset the aircraft weight, and will still be operating at an L/D of 21.2. Interference between the wing and rotor is not modeled in this study. In a similar study by Moodie and Yeo, interference effects were shown to increase the total power by less than 1% (Ref. 21). The effects of aileron deflections are included in the aerodynamic coefficient tables for the Aerostar FJ-100 wing for up to 10° of differential.

The propeller thrust is modeled as a point force (parallel to the waterline of the aircraft) and a yaw moment (parallel to the rotor torque vector), which are applied in line with the vertical coordinate of the center of gravity, and at the quarter-chord of the wings longitudinally. This is done so that the collective propeller thrust acts only in the longitudinal body direction without producing a coupled pitching moment. The magnitude of the thrust and the yaw moment are directly prescribed as controls. Propeller power is determined in post processing using a blade element vortex theory (BEVT) model of two pitch controlled four-bladed propellers with a 4.5 ft radius at 1,934 RPM.

The horizontal stabilizer is modeled after the size and location of the UH-60A stabilizer, with airfoil coefficients interpolated from a table of NACA 0012 wind tunnel data. Interference between the wake of the rotor and the horizontal tail is neglected.

To simulate the inflow in hover, a 12×12 Peters-He dynamic inflow model is used (Ref. 35). A dual core prescribed wake model is selected to model the inflow in forward flight, which captures the effects of producing negative lift on the advancing tip of the blade.

The simulations are produced using the US Army's Rotorcraft Comprehensive Analysis System (RCAS), version 15.09 (Ref. 36). The structural and aerodynamic models are built to the above mentioned specifications in RCAS using 13 elastic beam elements, 36 aerodynamic sections, and an azimuthal resolution of 5° for calculation of airloads. The flap and lag hinges, and pitch bearings are modeled as torsional spring/damper elements, and pitch control is prescribed through a spring element with a stiffness that is representative of the pitch link and swashplate stiffness of a UH-60A. As a computational tool, the RCAS UH-60A structural model has been validated against UH-60A flight test data (Ref. 37), and the prescribed wake model has been validated against wind tunnel test data of an untwisted H-34 rotor at advance ratios up to 0.46 (Ref. 38).

MODEL SELECTION

Surrogate modeling is a strategy which replaces experimental measurements and/or computationally expensive physics based simulations with low order modeling or curve fit approximations in order to improve the speed of predictions at an acceptable level of accuracy. It is commonly used in design optimization studies with a large number of design variables, where gradient based methods on the full model would take an inordinate amount of time (Refs. 39–41).

The study in Ref. 33 demonstrated how surrogate modeling could also be applied to the problem of control redundancy for a compound helicopter. In hover, quadratic regression was used to produce a model of power as a function of collective propeller thrust and main rotor speed. It was demonstrated that when the regression was performed on a large dataset (105 trim states), the model could accurately predict the combinations of control settings that produced the minimum power hover trim state. Using 416 trim states at 100 kts, a second model was produced to predict power as a function of collective propeller thrust, main rotor speed, and stabilator pitch. The second model suffered from inaccuracies for combinations of low rotor speed and low collective propeller thrust, where the blade pitches entered a dynamic stall regime and the power could not be well represented as a quadratic combination of controls.

For this paper, a significantly larger range of flight speeds are considered, with parametric variations in collective propeller thrust, main rotor speed, and stabilator pitch performed at each flight speed. The ranges and increments used for each control and flight speed are summarized in Table 2. The second column of Table 2 gives the total number of feasible trim

Table 2. Parametrically varied controls and resulting power ranges at each flight speed

V (kts)	states	Ω (rad/s)	T_{coll} (lbs)	δ_s (deg)	P (hp)
0	74*	22 – 27	−3000 – 3000	0*	2,323 – 2,808
50	855	20 – 27	0 – 6000	−18 – 18	1,067 – 2,718
100	780	17 – 27	0 – 6000	−18 – 18	785 – 3,818
in increments of:		*1*	*500*	*3*	
150	372	19 – 27	0 – 3500	−6 – 12	1,401 – 3,329
in increments of:		*1*	*250*	*3*	
200	106	18 – 25	2250 – 4500	−1.5 – 6	2,887 – 4,411
in increments of:		*1*	*250*	*1.5*	

**duplicated at $\delta_s = \pm 18°$, for 222 states total*

states that were produced through the parametric variations, subject to the constraints in Table 3, and the implicit constraint of achievable steady level flight. Because stabilator dynamic pressures are assumed to be zero in hover, the 74 states with 0° stabilator pitch are reproduced for stabilator pitches of −18° and 18°—for a total of 222 trim states in hover and 2,335 trim states across all flight speeds.

In order to develop a unified model, which includes flight speed as a predictor (for a total of four inputs to the surrogate model), artificial neural network modeling will be used. The artificial neural network model used in this study is a single hidden layer of neurons, with each neuron connected to every input node, and every output node, as seen in Figure 2. Each hidden layer neuron multiplies a vector of the weights and a bias (Eqn. 1) by the nodes of the input layer (Eqn. 2), and uses the hyperbolic tangent sigmoid transfer function described in Eqn. 3 to produce the hidden layer output at each node. The output layer gives the estimated power as a linear combination of the hidden layer outputs and an additional bias. The total number of model coefficients grows linearly with the size of the hidden layer ($6n+1$). By increasing the size of the hidden layer, the sophistication of the network increases, and it can model more complex relationships accurately (Ref. 42).

$$W_{in}^n = \begin{bmatrix} w_\Omega^n & w_{T_{coll}}^n & w_{\delta_s}^n & w_V^n & b^n \end{bmatrix} \tag{1}$$

$$H_{in}^n = W_{in}^n \cdot \begin{bmatrix} \Omega & T_{coll} & \delta_s & V & 1 \end{bmatrix}^T \tag{2}$$

$$H_n^{out} = \frac{2}{1+e^{-2(H_{in}^n)}} - 1 \tag{3}$$

$$W_n^P = \begin{bmatrix} w_1^P & w_2^P & \dots & w_n^P & b^P \end{bmatrix} \tag{4}$$

$$P = W_n^P \cdot \begin{bmatrix} H_1^{out} & H_2^{out} & \dots & H_n^{out} & 1 \end{bmatrix}^T \tag{5}$$

For model comparison, the parametrically obtained trim state data is subdivided into a 70% training subset, 15% validation subset, and 15% testing subset. Over an epoch of training, the weights of the connections (the variables in Eqn. 1 and 4) are adjusted to reduce the sum of the squared error between the training subset and the model using Levenberg-Marquardt back-propagation. Training is complete when the error in the validation subset no longer decreases, which prevents overfitting the model to the training data. For model selection, neural network error was measured by performing 20 Monte-Carlo cross-validation iterations, with the training data randomly subdivided as previously described to find the average error between the model predictions and the testing subset.

Table 3. UH-60A main rotor control and flapping limits

Rotor Condition	Limits
Collective Pitch	$0.4° \leq \theta_0 \leq 16.4°$
Lateral Cyclic Pitch	$-8° \leq \theta_{1c} \leq 8°$
Longitudinal Cyclic Pitch	$-16° \leq \theta_{1s} \leq 16°$
Blade Flapping Angle	$-6° \leq \beta \leq 22°$
Adv. Tip Mach No.	$M_{tip} \leq 0.89$

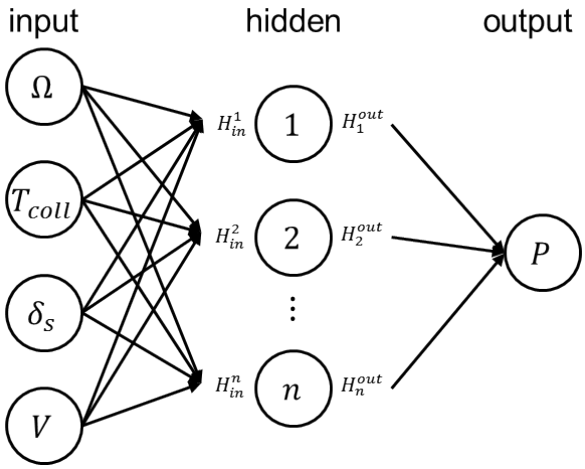

Fig. 2. Neural network architecture

Figure 3 compares the root mean square error in total power between quadratic regression, cubic regression, and the artificial neural network of increasing hidden layer size. The quadratic regression model has a root mean squared error of 168 hp, and the cubic regression model has a root mean squared error of 134 hp. Once it exceeds four neurons in the hidden layer, the neural network outperforms the cubic regression model. Further increasing the number of neurons in the hidden layer reduces the modeling error to 54 hp between 100

and 150 neurons, after which point there is a slight increase in error as the model begins to over-fit the true behavior of power. An appropriately sized neural network is capable of providing power estimates with about 60% – 70% less error than a 2^{nd} or 3^{rd} order polynomial regression fit model.

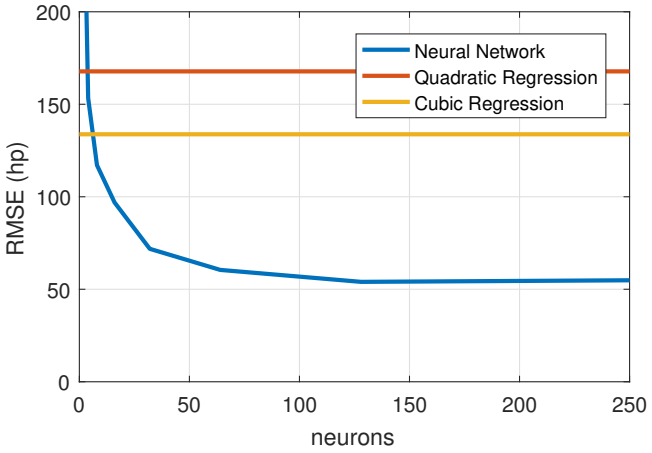

Fig. 3. Monte-Carlo cross validation showing variation in neural network power modeling error (hp) with increased hidden layer size compared to polynomial regression fit

Based on these observations, an artificial neural network with a single hidden layer of 150 neurons is chosen as the surrogate model. Figure 4 demonstrates how well neural networks can predict four of the control constraints from Table 3 using the same four inputs as the model in Figure 2. The best sized models for the constraint estimation appear to be between 50 and 150 neurons, with expected errors of between 0.25° and 0.5°.

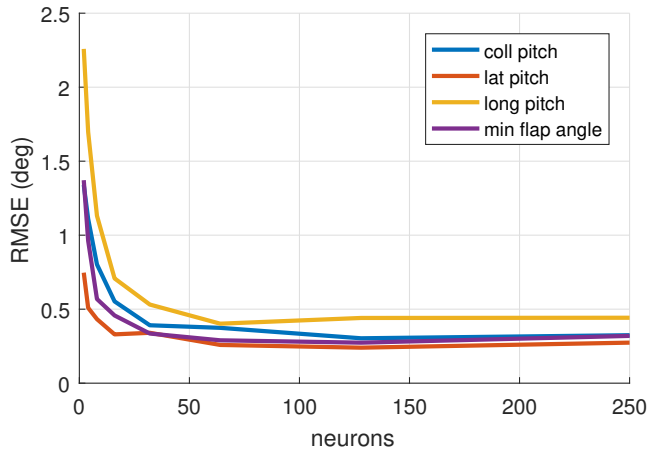

Fig. 4. Monte-Carlo cross validation showing variation in neural network modeling error with increased hidden layer size for optimization constraints (deg)

In the following section, a total of five models will be used to approximate the total power requirement, collective pitch, lateral cyclic pitch, longitudinal cyclic pitch, and minimum flapping angles in response to variations in flight speed, main rotor speed, collective propeller thrust, and stabilator pitch.

ALLOCATION FOR MINIMUM POWER

At each flight speed, the redundancy of control allows the pilot of a compound helicopter to produce trim using only a subset of the controls available to them. In hover and low flight speeds a compound helicopter would be expected to fly similarly to a conventional helicopter, due to the absence of high dynamic pressures on the wings and stabilator control surfaces. A pilot trimming the aircraft in this flight regimes may only use the conventional main rotor controls—setting the main rotor speed to its nominal value (27 rad/s) and the collective propeller thrust to 0 lbs. From the parametric analysis performed, this trim state is known to have a power requirement of 2,355 hp. Parametric analysis also demonstrated that a lower rotor speed (23 rad/s), and slightly positive collective propeller thrust (500 lbs) would produce a 32 hp reduction in power requirement of 2,323 hp.

For the full model, a set of five neural networks with 150 neurons in the hidden layer are trained on a random selection of 80% of the RCAS simulation dataset, while the remaining 20% is used for validation. Figure 5 shows a comparison of the parametric trim sweep determined power requirements to artificial neural network predictions of power in hover with stabilator pitch set to 0°. There is a good qualitative agreement between the predictions and the RCAS simulations on which they were trained, with a high sensitivity to change in collective propeller thrust, and a low sensitivity to change in rotor speed. The lack of feasible RCAS trim data for combinations of low rotor speed and highly negative collective propeller thrust is captured by the neural network as a violation of the maximum collective pitch limit of the rotor.

By performing a constrained optimization, the artificial neural networks could be used to inform a pilot of the optimal combination of unused controls that can be used to minimize power in trim for any given flight speed. The optimization can be performed rapidly, and delivers near-instantaneous results. In hover, the neural network prediction for minimum power allocates the collective propeller thrust to 71 lbs, and the main rotor speed to 23.7 rad/s, as shown in the first line of Table 4. The output of the neural network with this combination of controls predicts a power of 2,309 hp. By setting the redundant controls to these values and using RCAS to produce a new trim states, it was found that the neural network allocated controls had a true trim requirement of 2,323 hp. The RCAS simulated neural network minimum is detailed in Table 5 and compared side by side against the parametric variations in Figure 5. The modeling error of the neural network is 14 hp, but the allocation of controls is still capable of producing a trim state with the same power as the minimum obtained through parametric variation. At the minimum power in Figure 5, there is a large low-power region, which shows that it is fairly tolerant to errors in the allocated controls.

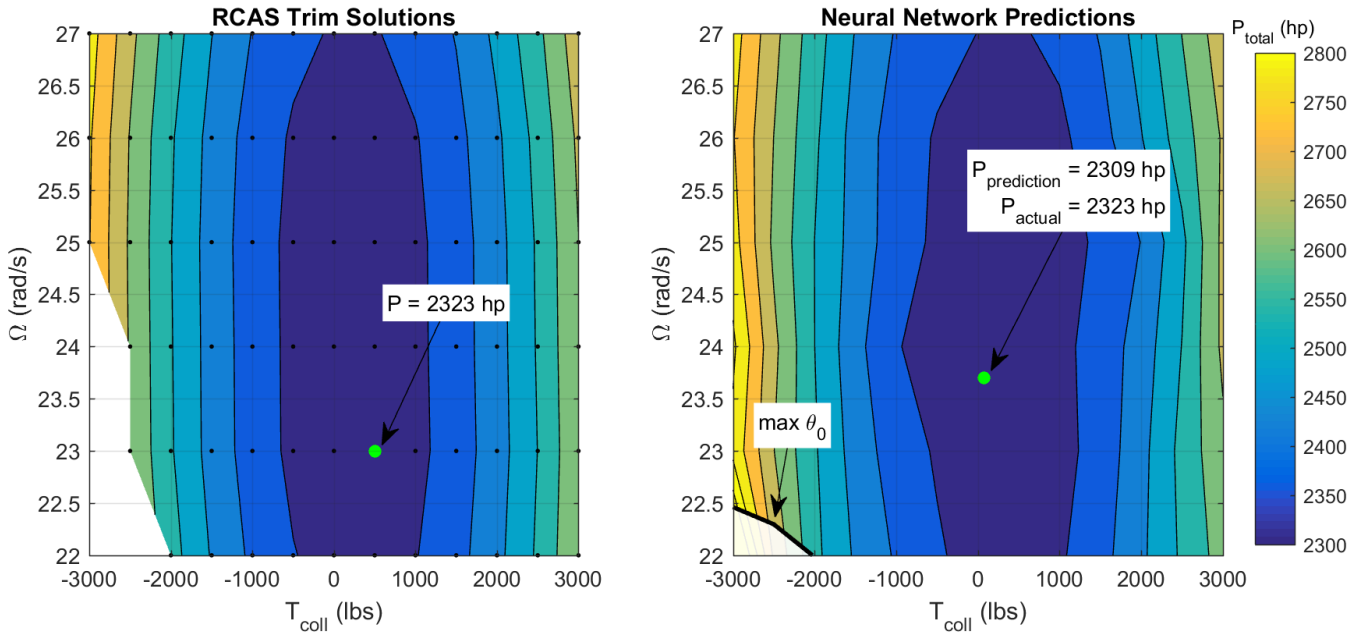

Fig. 5. Comparison of RCAS to neural network predictions of power (hp) in hover, showing minimum power trim states

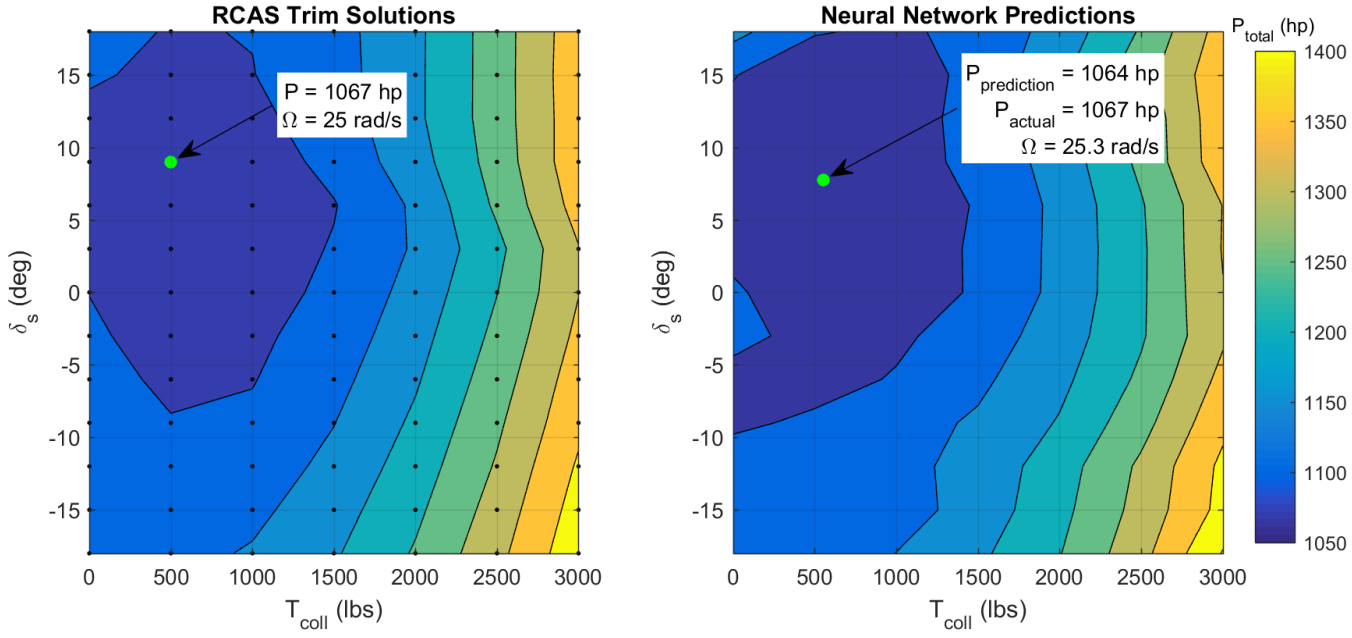

Fig. 6. Comparison of RCAS to neural network predictions of power (hp) at 50 kts, showing minimum power trim states

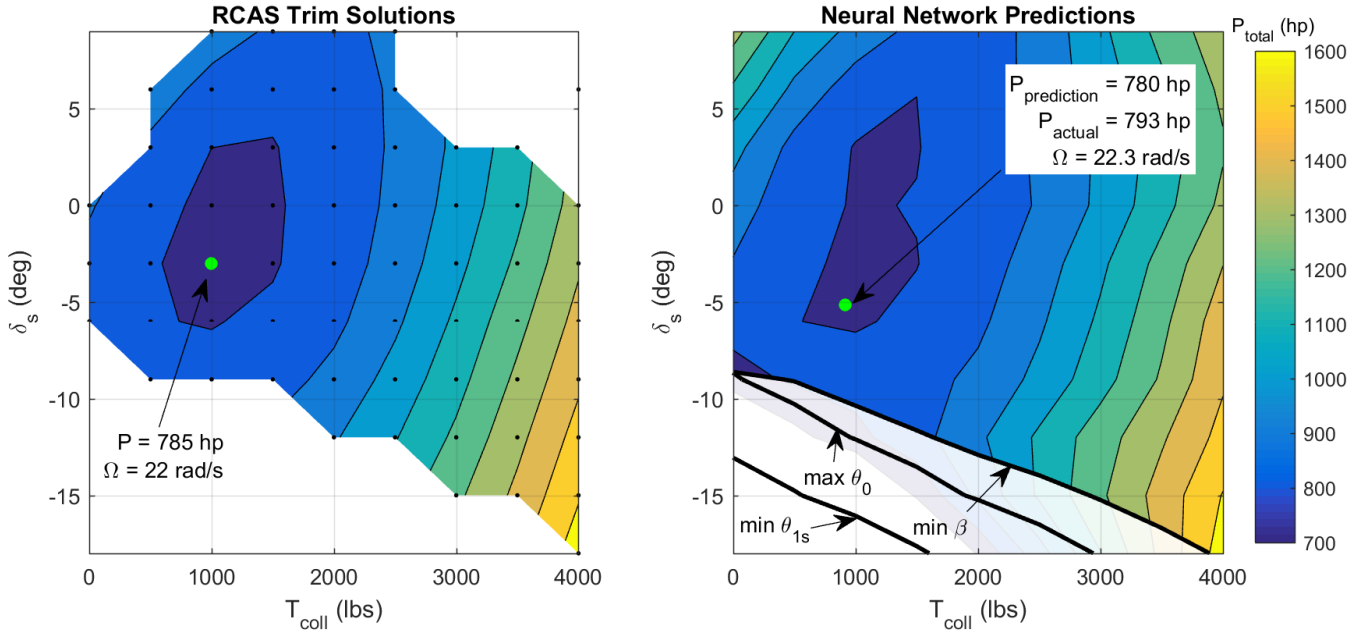

Fig. 7. Comparison of RCAS to neural network predictions of power (hp) at 100 kts, showing minimum power trim states

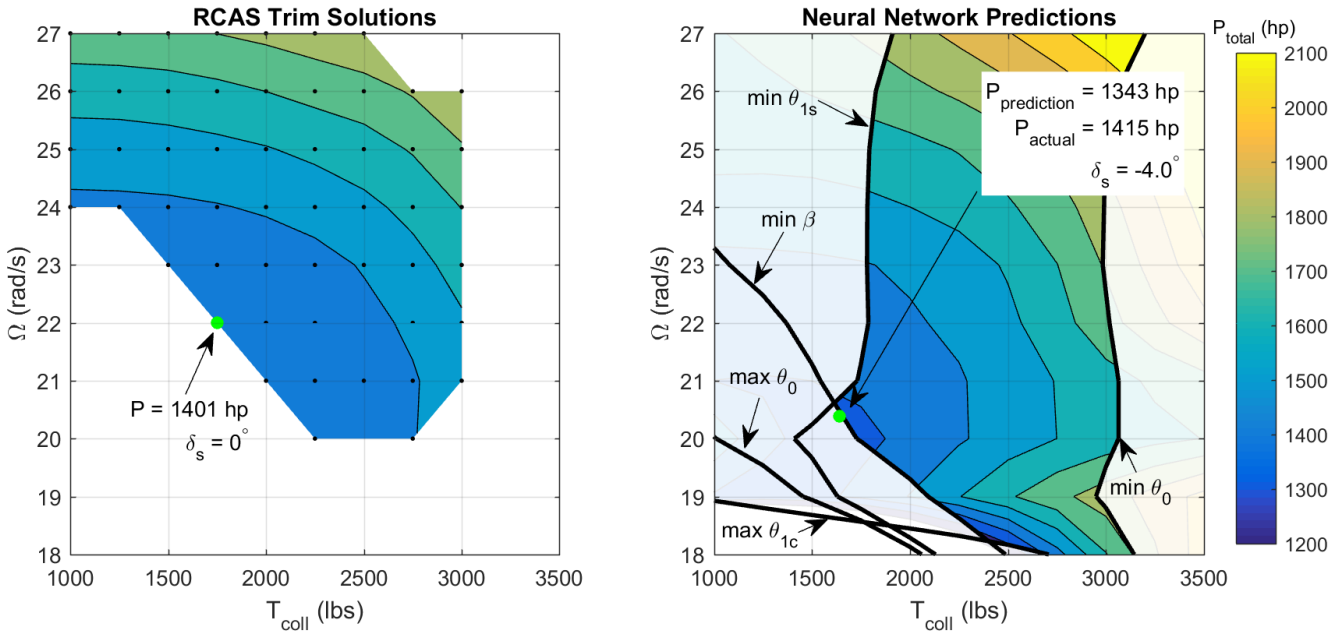

Fig. 8. Comparison of RCAS to neural network predictions of power (hp) at 150 kts, showing minimum power trim states

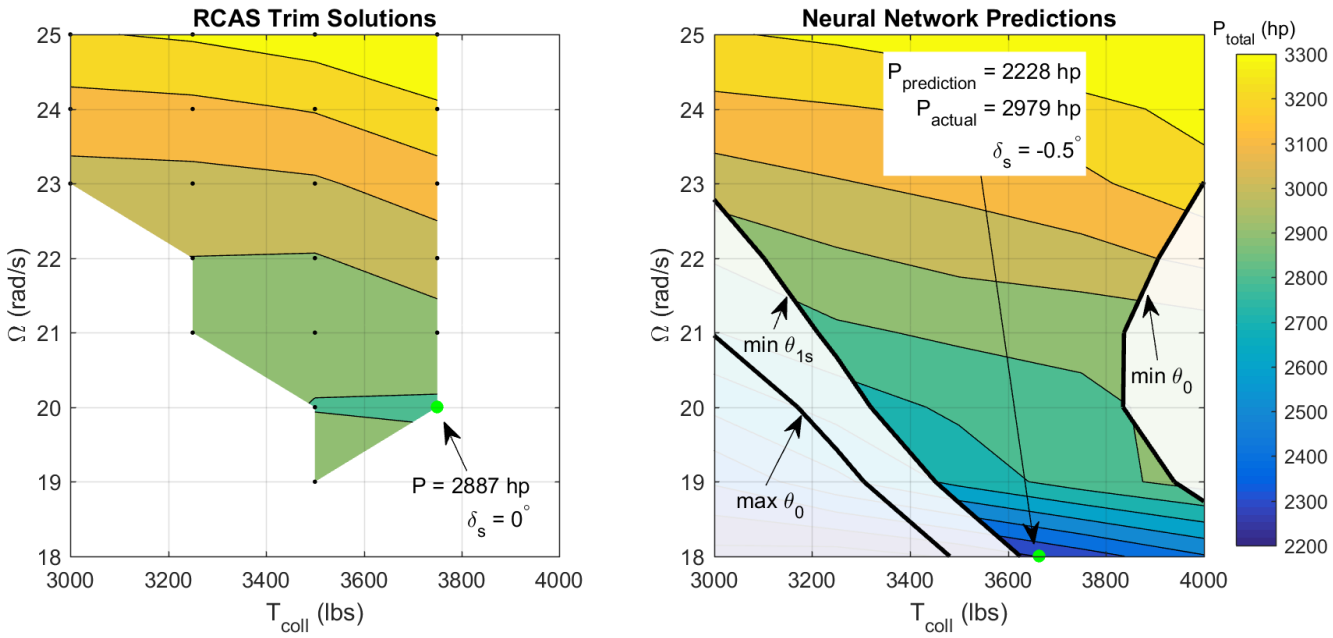

Fig. 9. Comparison of RCAS to neural network predictions of power (hp) at 200 kts, showing minimum power trim states

Table 4. Control allocation for minimum power

V (kts)	P (hp)	Ω (rad/s)	T_{coll} (lbs)	δ_s (deg)
RCAS parametric variations				
0	2,323	23	500	0
50	1,067	25	500	9
75	782	22	1,000	0
100	785	22	1,000	−3
150	1,401	22	1,750	0
200	2,887	20	3,750	0
Neural network predictions (powers are estimates)				
0	2,309	23.7	71	0
50	1,064	25.3	552	7.8
75	681	20.5	1,442	−5.0
100	780	22.3	918	−5.1
150	1,343	20.4	1,639	−4.0
200	2,228	18.0	3,664	−0.5

The same process is repeated at 50 kts in Figure 6. At this speed, stabilator pitch has a non-zero sensitivity in the RCAS simulations, so the comparison is made over collective propeller thrust and stabilator pitch variation for constant slices of rotor speed. Every point in the RCAS trim solution contour plot corresponds to a rotor speed of 25 rad/s, and every point in the neural network prediction contour plot corresponds to a slightly higher 25.3 rad/s. As shown in Table 4, these are the respective values associated with the minimum powers. Similarly to the hover case, the neural network predicts that it will achieve a slightly lower power with this combination of redundant controls, but by simulating this minimum in RCAS, it is found to have 3 hp of modeling error. The actual power requirement using the neural network allocated controls is the same as the parametrically found minimum, at 1,067 hp.

Table 5. RCAS runs with neural network allocated controls for minimum power

V (kts)	P (hp)	θ_0	θ_{1c}	θ_{1s}	min flap
0	2,323	14.0	0.7	−6.4	−1.2
50	1,067	8.7	1.3	−5.9	0.6
75	954	10.2	2.4	−11.1	−0.3
100	793	8.1	0.6	−11.1	−3.0
150	1,415	10.0	−0.1	−15.5	−5.8
200	2,979	12.7	−0.9	−16.3	−3.8

Figure 7 shows similar slices for the 100 kts power. When simulated in RCAS, the neural network allocated controls at 100 kts produce a trim state with 793 hp, which is higher than the parametrically found minimum by 1%. In the RCAS trim solution plot, there are areas where the trim solutions were unable to converge, or produced solutions that violated the constraints in Table 3. The artificial neural network model of blade flapping predicts that for highly negative stabilator pitches, the blade flapping angle will exceed the −6° minimum. The area of the contour plot that is bounded by that constraint in the neural network plot is equivalent to the lower edge of the RCAS trim solutions contour plot. Trimmed solutions found in this space during parametric variation were omitted for exceeding the minimum blade flapping angle, which shows agreement between the simulations and the neural network model.

At 150 kts the modeling of the minimum flapping constraint becomes relevant to the minimum power prediction, as the flapping constraint is active at neural network optimum in Figure 8. This trim state is found with a rotor speed of 20.4 rad/s,

collective propeller thrust of 1,639 lbs, and −4.0° of stabilator pitch—as described in Table 4. The RCAS trim solution contour plot shows that the parametrically found minimum also lies right on the boundary of feasibility, but with a 1.6 rad/s higher rotor speed, and 4° higher stabilator pitch. At the higher rotor speed shown by the RCAS contour plot, the minimum longitudinal pitch constraint does not appear to prevent trim for lower rotor thrusts. Table 5 shows that the neural network predicted state trims with −15.5° of longitudinal flapping and a −5.8° minimum flapping angle, showing good agreement with the active constraints used in optimization. The neural network predicts a minimum power of 1,349 hp, but for the allocated combination of controls the actual power is 1,415 hp. The modeling error has increased significantly, to 66 hp, but when allocated the power is still within 1% of the parametrically determined minimum. In the absence of constraint modeling, the optimization routine would have driven the solution to much lower collective propeller thrusts and rotor speeds, which would have produced infeasible trim states.

In Figure 9 the neural network allocation of controls for minimum power at 200 kts is constrained by minimum longitudinal pitch and minimum rotor speed. Compared to the RCAS minimum trim solution, this point is has a 0.5° lower stabilator pitch, 2 rad/s lower rotor speed, and 86 lbs less collective propeller thrust. The power of the neural network allocated solution is 3% higher than the minimum of the training data, but in Table 5 the actual longitudinal cyclic pitch violates the constraint by 0.3°. As the rotor speed decreases and the flight speed increases, the high advance ratio results in reduced authority of the main rotor controls. The trimmed aircraft thus requires larger pitch angles to produce the same forces and moments it could at higher rotor speeds, resulting in an increased sensitivity of the blade pitches to redundant control variation. This effect contributes to larger modeling errors at high advance ratios.

Relative to the large minimum power regions in Figures 5, 6, and 7, power appears to have a higher sensitivity to change in the redundant controls at higher speeds, signifying a greater penalty to lack of power modeling accuracy. Of equal importance is the constraint modeling, which are necessary to prohibit infeasible trim solutions, while refraining from unnecessarily restricting lower power solutions from the optimal region. As can be seen in Figure 9, the neural network predicted minimum extrapolates to a combination of controls that is outside of the training dataset, and returns an infeasible solution. When extrapolating, the accuracy of the models suffers, which also contributes to an increased modeling error of 751 hp. For the neural network to be more accurate at these high speeds, a greater sampling density may be necessary. At lower speeds, the opposite is true, and a lower sampling density that was was provided could likely be tolerated without significant change to the allocated power.

Interpolation to 75 kts

By including flight speed as a predictor of power in the neural network, the model is capable of allocating controls for minimum power at any flight speed—including speeds at which no training points exist. To demonstrate this, Figure 10 shows the neural network predictions at 75 kts. The network was able to produce a minimum power trim state at both 50 kts and 100 kts to within 1% of the minimum found through parametric variation. Each of these speeds had large datasets produced at them, but for predictions at 75 kts, there is no training data withing 25 kts. With the lack of relevant training data at 75 kts, the accuracy of the neural network model can be expected to decline.

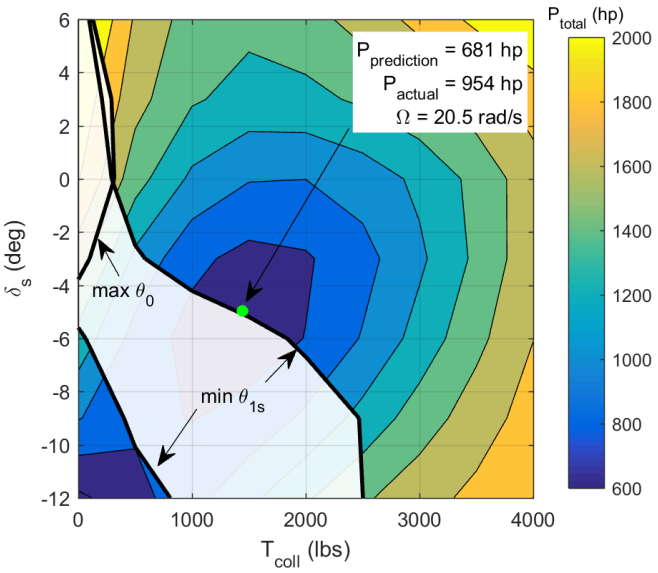

Fig. 10. Contour map at 75 kts of neural network power predictions (hp)

Tables 4 and 5 show the neural network predictions for 75 kts along with a brute force found approximate minimum, to the nearest 1 rad/s in rotor speed, 500 lbs in collective propeller thrust, and 3° of stabilator pitch. The minimum power predicted by the network is 681 hp for a combination of 20.5 rad/s of rotor speed, 1,442 lbs of collective propeller thrust, and −5° of stabilator pitch. When simulated, the modeling error is found to be 253 hp, about 7 times as much as the error at 100 kts, which demonstrates the importance of a high density set of training data in creating a globally accurate model. While typically neural network modeling error could be tolerated, since the controls given still produced low powers when simulated in RCAS, the actual power requirement is also 172 hp (22%) higher than the brute force minimum. Following trends in the columns of the RCAS minimums in Table 4 shows a fairly consistent trend of increasing collective propeller thrust and decreasing rotor speed from 50 – 200 kts. The same trends in the neural network predictions exist with exception to the 75 kts predictions, further demonstrating the error in the model.

MACHINE LEARNING ALGORITHM CASE STUDY

Most surrogate model optimization strategies use model updates after each successive function evaluation to improve the accuracy of the surrogate model and converge on a true minimum. Applying this strategy to compound helicopter power minimization should allow a targeted optimization to converge on a near-optimal power even with a very sparse set of training data. To test this hypothesis, a total of 20 training trim states are selected, five each at hover, 50 kts, 150 kts, and 200 kts. This will comprise the data used to train a model used to find the set of controls which minimize power at 100 kts. With such a small dataset, the 150 neuron neural networks used previously can be expected to be extremely over-fit. Figures 11 and 12 replicate the model selection cross validation using only 1% of the entire trim states data—with 16 trim states for training, 6 trim states for validation, and the remaining used to find the reported error. Due to the high number of possible permutations, the cross validations are performed 50 times, and the average root mean squared error (in hp and deg) are reported in Figures 11 and 12. Based on these figures, the hidden layer size is reduced to 8 neurons for the machine learning study.

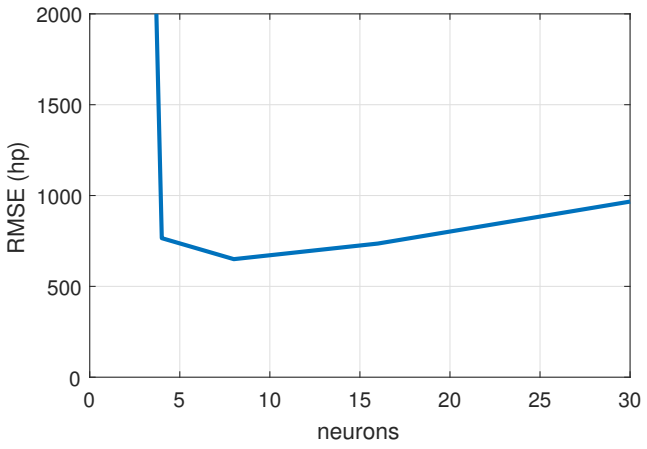

Fig. 11. Monte-Carlo cross validation showing variation in neural network power modeling error (hp) with increased hidden layer size trained on 23 trim states

Figures 11 and 12 can also be used to provide a benchmark for the level of modeling error to be expected in a neural network trained on such sparse data. With a root mean squared error of almost 700 hp, and 1° – 5° in the constraints, it can be expected that the initial modeling error will be excessive, and the allocation for minimal power will be be far from the 785 hp found through parametric analysis. Because of the stochastic nature of neural network training, two successive models—even when trained on the same data—can return vastly different predictions. To reduce this variation and produce a more accurate model, a set of 20 neural networks are trained, and the weighted average of their prediction is used as a collaborative model.

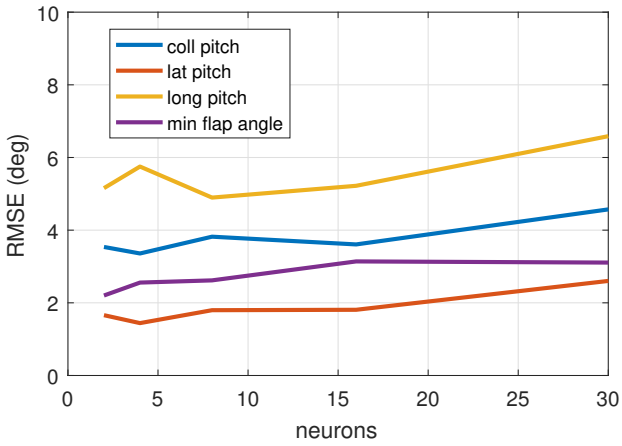

Fig. 12. Monte-Carlo cross validation showing variation in neural network modeling error with increased hidden layer size for optimization constraints (deg) trained on 23 trim states

Figure 13 shows the initial prediction at 100 kts for the model trained on 20 trim states. The first row of Table 6 summarizes the minimum of the model, showing that the modeling error in power is 691 hp, which corroborates the modeling error from Figure 11. When used to allocate the controls of an RCAS simulation, these control return a power of 1,579 hp, which is over 100% higher than the expected minimum from parametric variation.

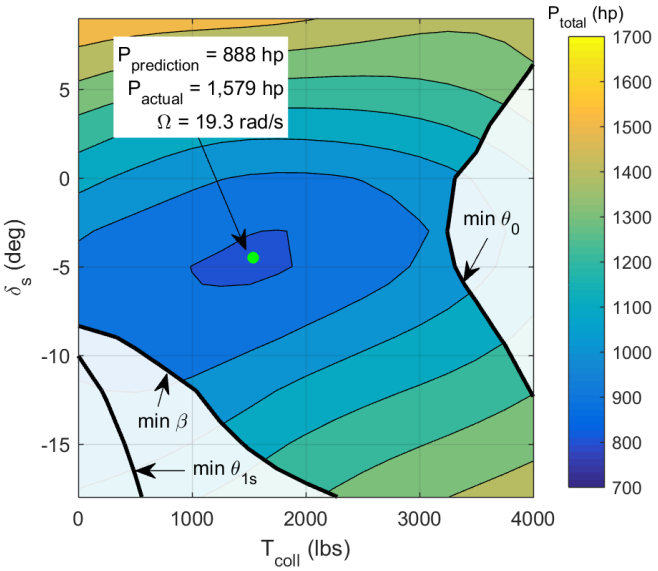

Fig. 13. Contour map at 100 kts of neural network power predictions (hp) for the 1st iteration of machine learning

Adding the trim state found in the first iteration and updating the model yields a large improvement in modeling error and in the power found from control allocation. Figure 14 shows how the evolution of the model tends to improve model min-

Table 6. Machine learning model progression

iteration	$P_{prediction}$ (hp)	P_{actual} (hp)	error (hp)	Ω (rad/s)	T_{coll} (lbs)	δ_s (deg)
1	888	1,579	691	19.3	1,536	−4.5
2	1,012	871	142	22.3	2,151	−1.5
3	884	1,009	125	22.4	2,878	1.1
4	975	854	121	21.9	2,143	0.2
5	862	857	5	22.5	2,085	0.7
6	864	862	1	22.4	2,153	1.4
7	918	827	92	23.1	1,904	−0.3
8	821	801	19	22.8	1,419	−0.4
9	800	798	2	23.1	919	0.4
10	829	793	36	22.4	1,555	0.0

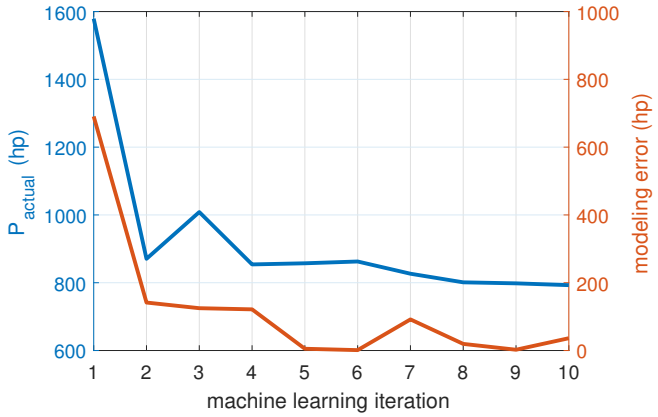

Fig. 14. Model development showing neural network predictions through machine learning iterations

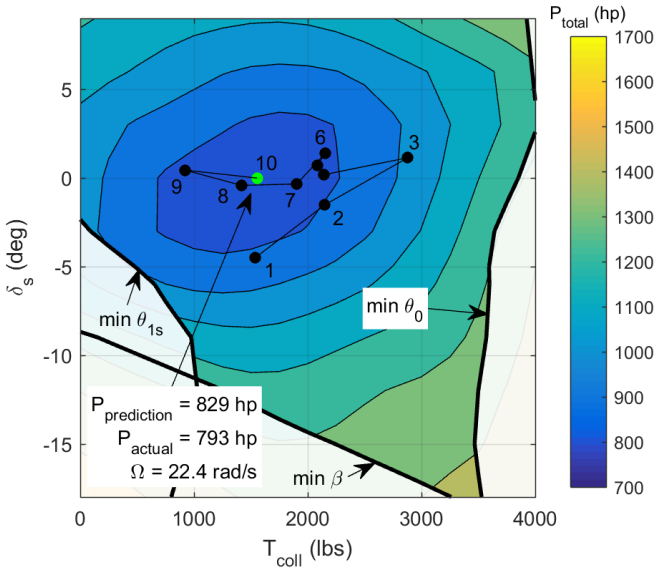

Fig. 15. Contour map at 150 kts of neural network power predictions (hp) for the 2nd iteration of machine learning

imum power predictive performance, and the modeling error in power at that minimum.

After 5 iterations of the machine learning algorithm, the modeling error is typically less than 50 hp at the allocated minimum, which is better than the root mean squared error of the 150 neuron network trained on the full dataset in Figure 3. This improvement in accuracy is due to the high concentration of training data in the immediate vicinity of the relevant combination of controls. For any predictions made away from this locality, the same errors from Figure 11 that were experienced in the first iteration can still be expected. Figure 15 shows the neural network predictions of power on the 10th iteration, with each of the 9 prior predictions marked. Compared to Figure 7, which is at approximately the same rotor speed, the power predictions in the immediate vicinity of the training points match reasonably well, but accuracy decreases considerably outside of this region. The differences are exemplified at high collective propeller thrusts, which are predicted to be infeasible due to minimum collective pitch according to the neural network in Figure 15, but is demonstrably not, according to the parametric trim sweep in Figure 7. Near the predicted minimum, the high density of training states (33% of the entire set) help bias the model to improve accuracy in this region, which results in an allocated minimum power of 793 hp, which is within 1% of the parametrically determined minimum.

Targeted machine learning updates to a model can converge upon a reasonably low power combination of redundant controls in under 10 iterations of trimming the aircraft and updating the model. After 10 iterations, Table 6 and Figure 14 show that the controls allocated by a model trained through machine learning can match those of a model trained with parametrically varied training data using 78 times as many training points. The machine learning training process, however, cannot be expected to perform as well outside of a highly local region.

CONCLUSIONS

This study presents a surrogate model based method of allocating the set of redundant controls present on a compound helicopter to produce a trim state with minimum power. An artificial neural network is trained with a comprehensive set of trim data for five flight speeds from hover to 200 kts.

Between hover and 100 kts, the model is shown to be able to allocate the three redundant controls (main rotor speed, collective propeller thrust, and stabilator pitch), such that trimming the aircraft using the conventional pilot controls yields a power requirement within 1% of the true minimum. At these speeds, modeling error is tolerated by a large, low power region that is not very sensitive to variations in the compound controls.

At flight speeds of 150 and 200 kts, the increased sensitivity of power to variations, and reduced size of the low power region necessitates higher modeling accuracy. Additionally, the high advance ratio characteristics of the main rotor require accurately modeling the main rotor control and flapping limits to avoid allocating redundant controls that cannot be feasibly trimmed by the main rotor. At 200 kts, constraint modeling error results in a neural network prediction that violates the minimum longitudinal pitch constraint.

Attempting to use the model to interpolate to an intermediary flight speed of 75 kts demonstrates the necessity of having training data near the predictions. With no training data within 25 kts, the allocated minimum at this flight speed requires a power that is 22% higher than the true minimum.

A sparse model is produced using only 20 randomly selected trim states to demonstrate a machine learning method of updating the model with new trim state data to improve accuracy and converge on the true minimum. Within 10 iterations, the machine learning model trained on only 30 trim states is capable of allocating controls for minimum power at 100 kts to the same level of accuracy as the 2,335 state comprehensive dataset.

Author contact: Jean-Paul Reddinger, reddij2@rpi.edu; Farhan Gandhi, fgandhi@rpi.edu

REFERENCES

[1]Leishman, J. G., *The Helicopter—Thinking Forward, Looking Back*, College Park Press, College Park, MD, 2007.

[2]Ruddell, A., "Advancing Blade Concept (ABC) Technology Demonstrator," U. S. Army Research and Technology Labotratories (AVRADCOM), USAAVRADCOM-TR-81-D-5, Apr. 1981.

[3]Bagai, A., "Aerodynamic Design of the X2 Technology^{TM} Demonstrator Main Rotor Blade," American Helicopter Society 64th Annual Forum, Montréal, QC, Canada, Apr. 29–May 1, 2008.

[4]Blackwell, R., and Millott, T., "Dynamics Design Characteristics of the Sikorsky X2 Technology^{TM} Demonstrator Aircraft," American Helicopter Society 64th Annual Forum, Montréal, QC, Canada, Apr. 29–May 1, 2008.

[5]Walsh, D., Weiner, S., Arifian, K., Bagai, A., Lawrence, T., and Blackwell, R., "Development Testing of the X2 Technology^{TM} Demonstrator," American Helicopter Society 65th Annual Forum, Grapevine, TX, May 27–29, 2009.

[6]Walsh, D., Weiner, S., Arifian, K., Lawrence, T., Wilson, M., Millott, T., and Blackwell, R., "High Airspeed Testing of the Sikorsky X2 Technology^{TM} Demonstrator," American Helicopter Society 67th Annual Forum, Virginia Beach, VA, May 3–5 2011.

[7]Colucci, F., "No Single Decision." *Vertiflite*, Nov./Dec. 2014: 10–11.

[8]Hirschberg, M., "Raider Rolls Out." *Vertiflite*, Nov./Dec. 2014: 12–13.

[9]Prouty, R. W., and Yackle, A. R., "The Lockheed AH-56 Cheyenne—Lessons Learned," AIAA-92-4278, AIAA Aircraft Design Systems Meeting, Hilton Head, SC, Aug. 24–26, 1992.

[10]Johnson, W., Yeo, H., and Acree, C. W., "Performance of Advanced Heavy-Lift, High-Speed Rotorcraft Configurations," AHS International Forum on Multidisciplinary Technology, Seoul, Korea, Oct. 15–17, 2007.

[11]Colucci, F., "SpeedHawk—Phase I." *Vertiflite*, Winter 2007.

[12]Nelms, D., "Aviation Week Flies Eurocopters X^3" *Aviation Week & Space Technology*, Vol. 174, No. 24, Jul. 9, 2012.

[13]Balmford, D. E. H., and Benger, B. S., "The Compound Helicopter—A Concept Revisited," 17th European Rotorcraft Forum, Berlin, Germany, Sept. 1991.

[14]Humpherson, D. V., "Compound Interest—A Dividend for the Future, Revised," American Helicopter Society 54th Annual Forum, Washington DC, May 2022, 1998.

[15]Orchard, M. N., and Newman, S. J., "The Compound Helicopter Versus Tilt Rotor—Europes Shortcut to the Future," 26th European Rotorcraft Forum, The Hague, Netherlands, Sept. 2000.

[16]Yeo, H., and Johnson, W. "Optimum Design of a Compound Helicopter," Presented at the Heli Japan 2006 AHS International Meeting on Advanced Rotorcraft Technology and Life Saving Activities, Nagoya, Japan, Nov. 2006.

[17]Yeo, H., and Johnson, W., "Aeromechanics Analysis of a Heavy Lift Slowed-Rotor Compound Helicopter," *Journal of Aircraft,* Vol. 44, (2), Mar./Apr. 2007, pp. 501–508.
doi: 10.2514/1.23905

[18]Floros, M. W., and Johnson, W., "Performance Analysis of the Slowed-Rotor Compound Helicopter Configuration," Vol. 54, (2), Apr. 2009, pp. 1–12.
doi: 10.4050/JAHS.54.022002

[19]Ormiston, R. A., "Low-Disk Loading Compound Rotorcraft for High Speed and Aerodynamic Efficiency," AHS, AIAA, SAE, RAeS International Powered Lift Conference Proceedings, Philadelphia, PA, Oct. 5–7, 2010.

[20]Hall, K. C., and Hall, S. R., "A Variational Method for Computing the Optimal Aerodynamic Performance of Conventional and Compound Helicopters," Vol. 55, (4), Oct. 2010, pp. 1–16.
doi: 10.4050/JAHS.55.042006

[21]Moodie, A. M., and Yeo, H., "Design of a Cruise-Efficient Compound Helicopter," *Journal of the American Helicopter Society,* Vol. 57, (3), Jul. 2012, pp. 1–11.
doi: 10.4050/JAHS.57.032004

[22]Rand, O., and Khromov, V., "Compound Helicopter: Insight and Optimization," *Journal of the American Helicopter Society,* Vol. 60, (1), Jan. 2015, pp. 1–12.
doi: 10.4050/JAHS.60.012001

[23]Datta, A., Yeo, H., and Norman, T. R., "Experimental Investigation and Fundamental Understanding of a Full-Scale Slowed Rotor at High Advance Ratios," *Journal of the American Helicopter Society,* Vol. 58, (2), Apr. 2013, pp. 1–12.
doi: 10.4050/JAHS.58.022004

[24]Sekula, M. K., and Gandhi, F., "Effects of Auxiliary Lift and Propulsion on Helicopter Vibration Reduction and Trim," *Journal of Aircraft,* Vol. 41, (3), May–Jun. 2004, pp. 645–656.
doi: 10.2514/1.496

[25]Gandhi, F., and Sekula, M. K., "Helicopter Vibration Reduction using Fixed-System Auxiliary Moments," *AIAA Journal,* Vol. 42, (3), Mar. 2004, pp. 501–512.
doi: 10.2514/1.575

[26]Sekula, M. K., and Gandhi, F., "Helicopter Vibration and Rotor Power Reduction through Horizontal Tail Incidence Angle Control," American Helicopter Society 60^{th} Annual Forum, Baltimore, MD, Jun. 7–10, 2004.

[27]Gandhi, F., and Sekula, M. K., "Helicopter Horizontal Tail Incidence Control to Reduce Rotor Cyclic Pitch and Blade Flapping," American Helicopter Society 60^{th} Annual Forum, Baltimore, MD, Jun. 7–10, 2004.

[28]Reddinger, J. P., and Gandhi, F., "Performance and Hub Vibrations of an Articulated Slowed-Rotor Compound Helicopter at High Speeds," American Helicopter Society 71^{st} Annual Forum, Virginia Beach, VA, May 5–7, 2015.

[29]Reddinger, J. P., and Gandhi, F., "Physics-Based Trim Optimization of an Articulated Slowed-Rotor Compound Helicopter in High-Speed Flight," *Journal of Aircraft,* Vol. 52, No. 6 (2015), pp. 1756–1766.
doi: 10.2514/1.C032939

[30]Barron, H. M., Brentner, K, Horn, J. F., Ozdemir, G. T., and Thorsen, A. T., "Acoustic Analysis of Compound Helicopters with Trim Variations," American Helicopter Society 69^{th} Annual Forum, Phoenix, AZ, May 21–23, 2013.

[31]Ozdemir, G. T., Horn, J. F., and Thorsen, A., "In-Flight Multi-Variable Optimization of Redundant Controls on a Compound Rotorcraft," AIAA Guidance, Navigation, and Control Conference, Boston, MA, August 19–22, 2013.

[32]Ozdemir, G. T., and Horn, J. F., "Simulation Analysis of a Flight Control Law with In-Flight Performance Optimization," American Helicopter Society 68^{th} Annual Forum, Fort Worth, TX, May 1–3, 2012.

[33]Reddinger, J. P., and Gandhi, F., "Response Surface Estimation of Trim Controls for a Compound Helicopter with Control Redundancy," American Helicopter Society 72^{nd} Annual Forum, West Palm Beach, FL, May 17–19, 2016.

[34]Yeo, H., Bousman, W. G., and Johnson, W., "Performance Analysis of a Utility Helicopter with Standard and Advanced Rotors," *Journal of the American Helicopter Society,* Vol. 49, (3), Jul. 2004, pp. 250–270.
doi: 10.4050/JAHS.49.250

[35]Peters, D. A., and He, C. J., "Correlation of Measured Induced Velocities with a Finite-State Wake Model," *Journal of the American Helicopter Society,* Vol. 36, (3), Jul. 1991, pp. 59–70. doi: 10.4050/JAHS.36.59

[36]Saberai, H., Khoshlahjeh, M., Ormiston, R., and Rutkowski, M. "Overview of RCAS and Application to Advanced Rotorcraft Problems," AHS 4^{th} Decennial Specialists' Conference on Aeromechanics, San Francisco, CA, Jan. 21–23, 2004.

[37]Silbaugh, B., Kang, H., Floros, M., and Singh, R. "Investigation of RCAS–CAMRAD II UH60 Structural Dynamics Model Correlation," American Helicopter Society 70^{th} Annual Forum, Montréal, QC, Canada, May 21–23, 2014.

[38]Jain, R., Yeo, H., Ho, J. C., and Bhagwat, M. "An Assessment of RCAS Performance Prediction for Conventional and Advanced Rotor Configurations," American Helicopter Society 70^{th} Annual Forum, Montréal, QC, Canada, May 21–23, 2014.

[39]Glaz, B., Goel, T., Liu, L., Friedmann, P. P., and Haftka, R. T., "Multiple-Surrogate Approach to Helicopter Rotor Blade Vibration Reduction," *AIAA Journal*, Vol. 47, No. 1 (2009), pp. 271–282. doi: 10.2514/1.40291

[40]Glaz, B., Friedmann, P. P., Liu, L., Cajigas, J. G., Bain, J., and Sankar, L. N., "Reduced-Order Dynamic Stall Modeling with Swept Flow Effects Using a Surrogate-Based Recurrence Framework," *AIAA Journal*, Vol. 51, No. 4 (2013), pp. 910–921. doi: 10.2514/1.J051817

[41]Gogulapati, A., Friedmann, P. P., and Martins, J. R. R. A., "Optimization of Flexible Flapping-Wing Kinematics in Hover," *AIAA Journal*, Vol. 52, No. 10 (2014), pp. 2342–2354. doi: 10.2514/1.J053083

[42]Haas, D.J., Milano, J., and Flitter, L., "Prediction of Helicopter Component Loads Using Neural Networks,"*Journal of the American Helicopter Society,* Vol. 40, (1), Jan. 1995, pp. 72–82. doi: 10.4050/JAHS.40.72